Scaling of Spin Hall Angle in 3d, 4d, and 5d Metals from $Y_3Fe_5O_{12}$/Metal Spin Pumping

H. L. Wang,[1] C. H. Du,[1] Y. Pu,[1] R. Adur,[1] P. C. Hammel,[1,*] and F. Y. Yang[1,†]
[1]Department of Physics, The Ohio State University, Columbus, Ohio 43210, USA

(Received 23 September 2013; revised manuscript received 24 December 2013; published 15 May 2014)

We have investigated spin pumping from $Y_3Fe_5O_{12}$ thin films into Cu, Ag, Ta, W, Pt, and Au with varying spin-orbit coupling strengths. From measurements of Gilbert damping enhancement and inverse spin Hall signals spanning 3 orders of magnitude, we determine the spin Hall angles and interfacial spin mixing conductances for the six metals. The spin Hall angles largely vary as Z^4 (Z: atomic number), corroborating the role of spin-orbit coupling. Amongst the four 5d metals, the variation of the spin Hall angle is dominated by the sensitivity of the d-orbital moment to the d-electron count, confirming theoretical predictions.

DOI: 10.1103/PhysRevLett.112.197201 PACS numbers: 75.47.Lx, 61.05.cp, 75.70.Ak, 76.50.+g

Spin pumping from a ferromagnet (FM) into a nonmagnetic material (NM) provides a promising route toward energy-efficient spintronic devices. The inverse spin Hall effect (ISHE) in FM/Pt bilayers [1–13] is widely used for detecting spin currents generated by either ferromagnetic resonance (FMR) or a thermal gradient. The intense interest in spin pumping emphasizes the pressing need for quantitative understanding of ISHE in materials other than Pt [10]. To date, spin Hall angles (θ_{SH}) have been measured for several metals and alloys by spin Hall or ISHE measurements, mostly using metallic FMs [14]. Because of current shunting of the metallic FMs and potential confounding effects of anisotropic magnetoresistance (AMR) or the anomalous Hall effect (AHE), the reported values of θ_{SH} vary significantly, sometimes by more than 1 order of magnitude for the same materials [14]. Here we report a systematic study of FMR spin pumping from insulating $Y_3Fe_5O_{12}$ (YIG) films grown by sputtering [15–22] into six metals, Cu, Ag, Ta, W, Pt, and Au, that span a wide range in two key parameters: a factor of ~50 in spin-orbit coupling (SOC) strength [23] and more than 2 orders of magnitude variation in spin diffusion length (λ_{SD}) [4,24–26]. Because of their weak SOC and relatively long λ_{SD}, Cu and Ag present a significant challenge for ISHE detection of spin pumping. ISHE voltages (V_{ISHE}) exceeding 5 mV are generated in our YIG/Ta and YIG/W bilayers and here we report ~1 μV ISHE signals in YIG/Cu and YIG/Ag. The proximity effect in Pt [9,13] should lead to at most a μV-level contribution to the measured V_{ISHE} and can be ignored. The large dynamic range that this sensitivity provides enables quantitative determination of spin mixing conductances across the YIG/metal interfaces [5,12] and spin Hall angles of these metals.

The excellent structural quality of our epitaxial YIG films deposited on (111)-oriented $Gd_3Ga_5O_{12}$ (GGG) substrates by sputtering [15–22] is demonstrated by high-resolution x-ray diffraction (XRD). A representative θ–2θ scan of a 20-nm YIG film shown in Fig. 1(a) demonstrates phase purity and clear Laue oscillations, indicating high uniformity of the film. The out-of-plane lattice constant of the YIG film, $c = 12.393$ Å, is very close to the bulk value of 12.376 Å. The XRD rocking curve in Fig. 1(b) gives a full width at half maximum (FWHM) of 0.0092°, demonstrating the excellent crystalline quality of the YIG film. The atomic force microscopy (AFM) image in Fig. 1(c) reveals a smooth surface with a roughness of 0.15 nm. Figure 1(c) shows the x-ray reflectometry (XRR) spectrum of a YIG(34 nm)/Pt (4.1 nm) bilayer, which exhibits the superposition of two oscillation periods corresponding to the 34-nm YIG and 4.1-nm Pt layers. The fit to the XRR is in excellent agreement with the experimental scan, from which we extract a YIG/Pt interfacial roughness of 0.22 nm. The XRR spectra of the other five metals on YIG exhibit similar interfacial sharpness (see the Supplemental Material [27]). Figure 1(e) shows a representative FMR derivative absorption spectrum for a 20-nm YIG film taken by a Bruker electron paramagnetic resonance (EPR) spectrometer in a cavity at radio frequency (rf) $f = 9.65$ GHz and an input microwave power $P_{rf} = 0.2$ mW with an in-plane magnetic field H. The peak-to-peak linewidth (ΔH) is 11.7 Oe and we find the effective saturation magnetization $4\pi M_{eff} = 1786 \pm 36$ Oe from the angular dependence of the resonance field [28]. Since the magnetic anisotropy of YIG is small, this means the saturation magnetization $4\pi M_s$ is close to 1786 G, in good agreement with values reported for single crystal YIG [29]. All six YIG/metal bilayers reported here are made from the same 20-nm YIG film.

Our spin pumping measurements are carried out in the center of the EPR cavity on the six YIG/metal bilayers (~1.0 mm × 5 mm) at room temperature. A dc magnetic field $\boldsymbol{H}$ is applied in the xz plane and the ISHE voltage is measured across the ~5–mm long metal layer along the y axis, as illustrated in Fig. 1(f). At resonance, the precessing YIG magnetization ($\boldsymbol{M}$) transfers angular momentum to the conduction electrons in the metal. The resulting pure spin current $\boldsymbol{J}_s$ is injected into the metal along the z axis with spin polarization $\boldsymbol{\sigma}$ parallel to $\boldsymbol{M}$ and then converted to a

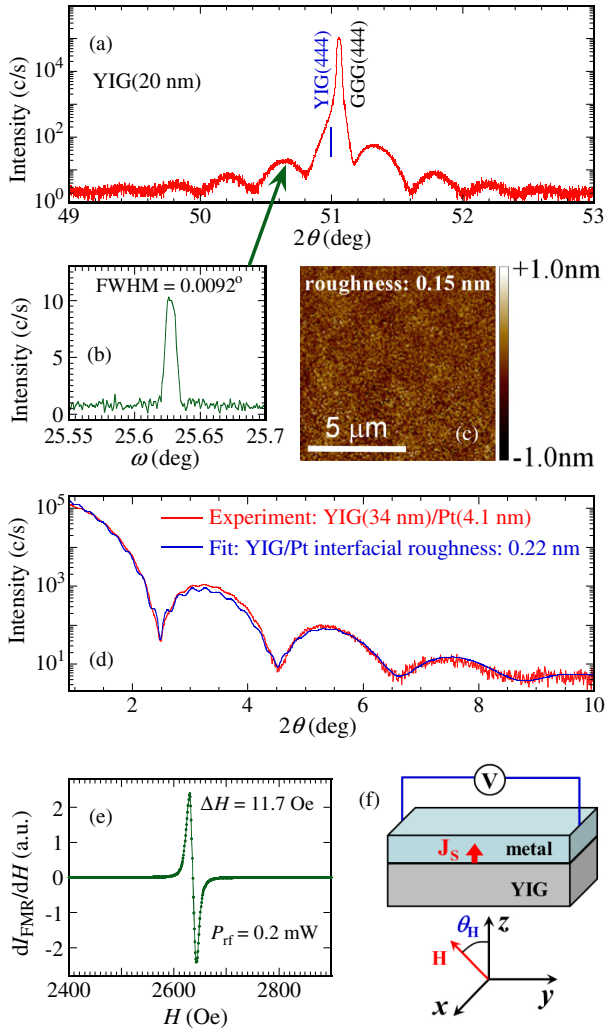

FIG. 1 (color online). (a) Semi-log θ–2θ XRD scan of a 20-nm thick YIG film near the YIG (444) peak (blue line), which exhibits clear Laue oscillations corresponding to the film thickness. (b) XRD rocking curve of the YIG film measured at $2\theta = 50.639°$ for the first satellite peak (green arrow) to the left of the main YIG (444) peak in (a) gives a FWHM of 0.0092°. (c) AFM image of a YIG film with a roughness of 0.15 nm. (d) X-ray reflectometry scan (red) of a YIG(34 nm)/Pt(4.1 nm) bilayer shows the superposition of oscillations from both the Pt and YIG layers. The fit (blue) to the experimental data gives a YIG/Pt interfacial roughness of 0.22 nm. (e) A representative room-temperature FMR derivative spectrum of a 20-nm YIG film with an in-plane field at $P_{rf} = 0.2$ mW, which gives a peak-to-peak linewidth of 11.7 Oe. (f) Schematic of experimental setup for ISHE voltage measurements.

charge current $\boldsymbol{J}_c \propto \theta_{SH}\boldsymbol{J}_s \times \boldsymbol{\sigma}$ by the ISHE via the SOC. The thickness of the metal layers is 5 nm for Ag, Ta, W, Pt, and Au and 10 nm for Cu. Resistivity (ρ) measurements confirm that the Ta and W films are β phase [30,31] (high resistivity, Table I).

Figure 2 shows V_{ISHE} vs H spectra of the six YIG/metal bilayers at $\theta_H = 90°$ and 270° (in-plane fields) at $P_{rf} = 200$ mW. For YIG/Ta and YIG/W bilayers, $|V_{ISHE}|$ exceeds 5 mV(1 mV/mm). For YIG/Pt, YIG/Au, and YIG/Ag, $V_{ISHE} = 2.10$ mV, 72.6 μV, and 1.49 μV, respectively. Because of the opposite signs of θ_{SH}, Pt, Au, and Ag give positive V_{ISHE} while Ta and W give negative V_{ISHE} at $\theta_H = 90°$, which agree with the predicted signs of θ_{SH} [32,33]. When $\boldsymbol{H}$ is reversed from $\theta_H = 90°$ to 270°, all the V_{ISHE} signals change sign as expected. The V_{ISHE} vs P_{rf} plots in the upper insets to Figs. 2(a)–2(f) show a linear dependence, indicating that the observed spin pumping signals are in the linear regime. Furthermore, we detect $V_{ISHE} = 0.99$ μV in the YIG/Cu bilayer [Fig. 2(f)]. Because of the weak SOC [24] in Cu, there is no previous report of ISHE detection of spin pumping in FM/Cu structures. This first observation of V_{ISHE} in YIG/Cu enables the determination of θ_{SH} in Cu.

When $\boldsymbol{H}$ is rotated from in-plane to out-of-plane, $\boldsymbol{M}$ remains essentially parallel to $\boldsymbol{H}$ at all angles since the FMR resonance field H_{res} (between 2500 and 5000 Oe) always exceeds $4\pi M_{eff}$ (1786 Oe). The lower insets to Figs. 2(a)–2(f) show the angular dependencies of the normalized V_{ISHE}; all clearly exhibit the expected sinusoidal shape ($V_{ISHE} \propto \boldsymbol{J}_s \times \boldsymbol{\sigma} \propto \boldsymbol{J}_s \times \boldsymbol{M} \propto \boldsymbol{J}_s \times \boldsymbol{H} \propto \sin\theta_H$). Since YIG is insulating we can rule out artifacts, such as AMR or AHE, enabling more straightforward measurement of the ISHE than using metallic FMs.

Figures 3(a)–3(f) show the FMR derivative absorption spectra ($f = 9.65$ GHz) of the 20-nm YIG films before and after deposition of the metals. The FMR linewidths are clearly enhanced in YIG/metal bilayers relative to the bare YIG films. The linewidth enhancement [10,11] is a consequence of spin pumping: the coupling that transfers angular momentum from YIG to the metal adds to the damping of the precessing YIG magnetization, thus increasing ΔH. In order to accurately determine the enhancement of Gilbert damping, we measure the frequency dependencies of ΔH for a bare YIG film and the six YIG/metal bilayers using a microstrip transmission line. In all cases, ΔH increases linearly with frequency [Fig. 3(g)]. The Gilbert damping constant α can be obtained using [34],

$$\Delta H = \Delta H_{inh} + \frac{4\pi\alpha f}{\sqrt{3}\gamma} \tag{1}$$

where ΔH_{inh} is the inhomogeneous broadening and γ is the gyromagnetic ratio. Table I shows the damping enhancement α_{sp} due to spin pumping: $\alpha_{sp} = \alpha_{YIG/NM} - \alpha_{YIG}$, where $\alpha_{YIG/NM}$ and $\alpha_{YIG} = (9.1 \pm 0.6) \times 10^{-4}$ are obtained from the least-squares fits in Fig. 3(g).

The ISHE voltages depend on several materials parameters [4,11],

$$V_{ISHE} = \frac{-e\theta_{SH}}{\sigma_N t_N + \sigma_F t_F}\lambda_{SD}\tanh\left(\frac{t_N}{2\lambda_{SD}}\right) g_{\uparrow\downarrow} f L P \left(\frac{\gamma h_{rf}}{2\alpha\omega}\right)^2 \tag{2}$$

TABLE I. ISHE voltages at $f = 9.65$ GHz and $P_{rf} = 200$ mW, FMR linewidth changes at $f = 9.65$ GHz, Gilbert damping enhancement due to spin pumping $\alpha_{sp} = \alpha_{YIG/NM} - \alpha_{YIG}$ ($\alpha_{YIG} = 9.1 \pm 0.6 \times 10^{-4}$), and resistivity of the six YIG/metal bilayers, and the calculated interfacial spin mixing conductance, spin Hall angle, and spin current density for each metal.

Bilayer	V_{ISHE}	ΔH change	α_{sp}	$\rho(\Omega m)$	$g_{\uparrow\downarrow}(m^{-2})$	λ_{SD}(nm)	θ_{SH}	$J_s(A/m^2)$
YIG/Pt	2.10 mV	24.3 Oe	$(3.6 \pm 0.3) \times 10^{-3}$	4.8×10^{-7}	$(6.9 \pm 0.6) \times 10^{18}$	7.3	0.10 ± 0.01	$(2.0 \pm 0.2) \times 10^{7}$
YIG/Ta	−5.10 mV	16.5 Oe	$(2.8 \pm 0.2) \times 10^{-3}$	2.9×10^{-6}	$(5.4 \pm 0.5) \times 10^{18}$	1.9	-0.071 ± 0.006	$(1.6 \pm 0.2) \times 10^{7}$
YIG/W	−5.26 mV	12.3 Oe	$(2.4 \pm 0.2) \times 10^{-3}$	1.8×10^{-6}	$(4.5 \pm 0.4) \times 10^{18}$	2.1	-0.14 ± 0.01	$(1.4 \pm 0.1) \times 10^{7}$
YIG/Au	72.6 μV	5.50 Oe	$(1.4 \pm 0.1) \times 10^{-3}$	4.9×10^{-8}	$(2.7 \pm 0.2) \times 10^{18}$	60	0.084 ± 0.007	$(7.6 \pm 0.7) \times 10^{6}$
YIG/Ag	1.49 μV	1.30 Oe	$(2.7 \pm 0.2) \times 10^{-4}$	6.6×10^{-8}	$(5.2 \pm 0.5) \times 10^{17}$	700	0.0068 ± 0.0007	$(1.5 \pm 0.1) \times 10^{6}$
YIG/Cu	0.99 μV	3.70 Oe	$(8.1 \pm 0.6) \times 10^{-4}$	6.3×10^{-8}	$(1.6 \pm 0.1) \times 10^{18}$	500	0.0032 ± 0.0003	$(4.6 \pm 0.4) \times 10^{6}$

where e is the electron charge, σ_N (σ_F) is the conductivity of the NM (FM), $t_N(t_F)$ is the thickness of the NM (FM) layer, $g_{\uparrow\downarrow}$ is the interfacial spin mixing conductance, $\omega = 2\pi f$ is the FMR frequency, L is the sample length, and $h_{rf} = 0.25$ Oe (see the Supplemental Material [27]) in our FMR cavity at $P_{rf} = 200$ mW. The factor P arises from the ellipticity of the magnetization precession [10],

$$P = \frac{2\omega[\gamma 4\pi M_s + \sqrt{(\gamma 4\pi M_s)^2 + 4\omega^2}]}{(\gamma 4\pi M_s)^2 + 4\omega^2} = 1.21. \quad (3)$$

$g_{\uparrow\downarrow}$ can be determined using [10–12],

$$g_{\uparrow\downarrow} = \frac{4\pi M_s t_F}{g\mu_B}(\alpha_{YIG/NM} - \alpha_{YIG}), \quad (4)$$

where g and μ_B are the Landé factor and Bohr magneton, respectively.

For Pt, Ta, and W with mV-level ISHE voltages, we measure λ_{SD} by varying their thicknesses and obtain

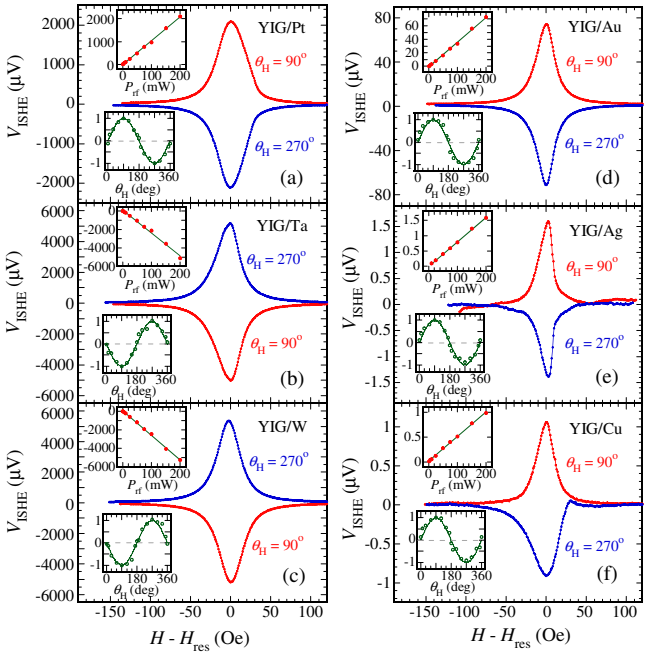

FIG. 2 (color online). V_{ISHE} vs H spectra of (a) YIG/Pt, (b) YIG/Ta, (c) YIG/W, (d) YIG/Au, (e) YIG/Ag, and (f) YIG/Cu bilayers at $\theta_H = 90°$ (red) and 270° (blue) using $P_{rf} = 200$ mW. Top insets: rf-power dependencies of the corresponding V_{ISHE} at $\theta_H = 90°$. Bottom insets: angular dependencies (θ_H) of V_{ISHE} normalized by the magnitude of V_{ISHE} at $\theta_H = 90°$, where the green curves are $\sin\theta_H$ for Pt, Au, Ag, Cu, and $-\sin\theta_H$ for Ta and W.

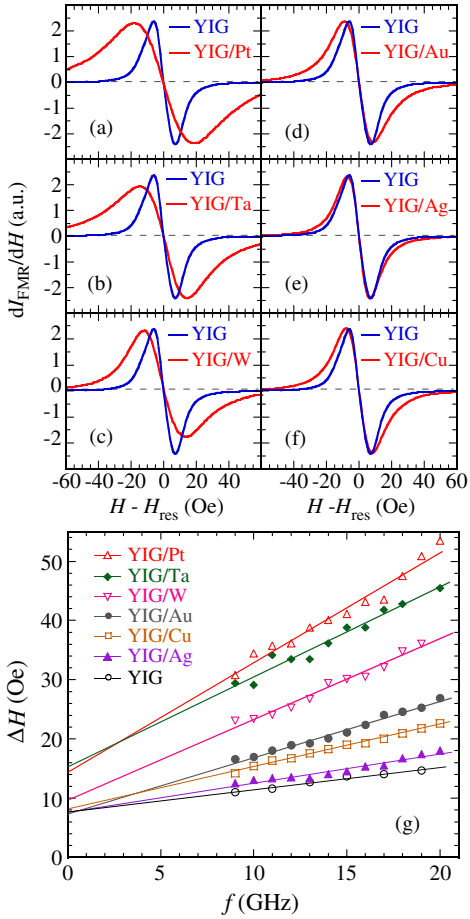

FIG. 3 (color online). FMR derivative absorption spectra of the 20-nm YIG films before (blue) and after (red) the deposition at $f = 9.65$ GHz of (a) Pt, (b) Ta, (c) W, (d) Au, (e) Ag, and (f) Cu. (g) Frequency dependence of peak-to-peak FMR linewidth of a bare YIG film and the six YIG/metal bilayers.

$\lambda_{SD} = 7.3$, 1.9, and 2.1 nm, respectively (see the Supplemental Material [27]), which agree with those reported in literature [4,25]. For Au, Ag, and Cu with much smaller V_{ISHE}, we use reported values of 60 nm for Au [24], 700 nm for Ag [26], and 500 nm for Cu [24]. Considering that the term $\lambda_{SD}\tanh(t_N/2\lambda_{SD})$ in Eq. (2) is essentially constant for $\lambda_{SD} > t_N$ due to the limitation of film thickness, variation in λ_{SD} does not affect the calculated values of θ_{SH} for the three noble metals [27]. Electrical conduction in YIG can be neglected. From Eqs. (2)–(4), $g_{\uparrow\downarrow}$ and θ_{SH} can be calculated, as shown in Table I [35]. Consequently, the spin current density J_s can be estimated using [11],

$$J_s = \frac{t_N\sigma_N + t_F\sigma_F}{\theta_{SH}\lambda_{SD}\tanh(\frac{t_N}{2\lambda_{SD}})}\frac{V_{ISHE}}{L}. \quad (5)$$

The power of ISHE as a probe of spin pumping calls for a quantitative understanding to enable more precise and detailed experiments. Spin Hall angles have been measured in several metals by spin Hall or ISHE measurements, mostly using metallic FMs [10,14,33,35]. Because of the impact of AMR or AHE in metallic FMs and the variation of sample characteristics among different groups, the reported values of θ_{SH} vary significantly for the same materials [14]. We have combined high sensitivity ISHE measurements with measurements of the spin-pumping enhancement of Gilbert damping of the insulating YIG film to determine θ_{SH} for various 3d, 4d, and 5d metals. This set of experimental data reveals trends and uncovers the roles of various materials parameters in SOC [23,32]. To probe the dependence of θ_{SH} on atomic number, we plot $|\theta_{SH}|$ vs Z^4 in Fig. 4(a). Except for W, all the other five metals roughly follow a linear dependence on Z^4: $\theta_{SH} = (Z/142)^4$, as expected given the central role of SOC [23]. The factor 142 indicates that, hypothetically, θ_{SH} would reach 1 at atomic number 142.

We note that among the four 5d metals, θ_{SH} varies significantly in both the sign and magnitude, suggesting that other factors, in particular, the d-electron count, also play important roles in the ISHE. Figure 4(b) shows θ_{SH} vs Z for Ta, W, Pt, and Au, which agrees well with the theoretical calculations of spin Hall conductivity (SHC), $\sigma_{SH} = [\hbar/2e]\theta_{SH}\sigma$ by Tanaka *et al.* [32], where σ is the electrical conductivity. Compared with previous theories that only consider atomic number in SOC [23], this calculation takes into account both atomic number and d-orbital configuration in the spin Hall effect. Our results provide experimental confirmation of the predicted important role of the d-electron count in spin Hall physics [32]. In addition, if one only looks at the data points of Cu, Ag, and Au in Fig. 4(a), they follow the Z^4 dependence very well, which highlights the key role of the atomic number in SOC, given that the three metals have the same d-electron count [23].

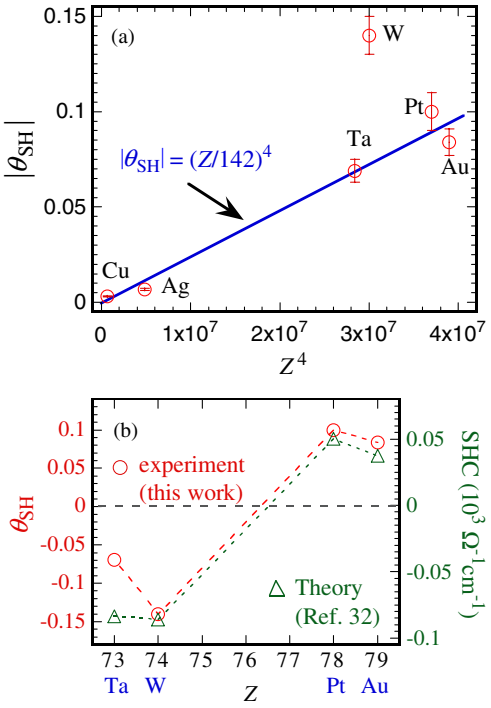

FIG. 4 (color online). (a) Absolute values of θ_{SH} as a function of Z^4 for the six metals. The blue line is the least-squares fit to five metals: Cu, Ag, Ta, Pt, and Au, which gives $\theta_{SH} = (Z/142)^4$. (b) Spin Hall angles (red circles) of the 5d transition metals Ta, W, Pt, and Au, of which both the signs and relative magnitudes agree well with the theoretical calculation (green triangles) of spin Hall conductivity in Ref. [32].

In conclusion, FMR spin pumping measurements give mV-level ISHE voltages in YIG/Pt, YIG/Ta, and YIG/W bilayers and robust ISHE signals in YIG/Cu and YIG/Ag. Interfacial spin mixing conductances are determined by the enhanced Gilbert damping. The inferred spin Hall angles of the six metals imply the important roles of atomic number and d-electron configuration in spin Hall physics.

This work is supported by the Center for Emergent Materials at the Ohio State University, a NSF Materials Research Science and Engineering Center (No. DMR-0820414) (H. L. W., Y. P., and F. Y. Y.) and by the U.S. Department of Energy through Grant No. DE-FG02-03ER46054 (R. A. and P. C. H.). Partial support is provided by Lake Shore Cryogenics Inc. (C. H. D.) and the NanoSystems Laboratory at the Ohio State University. H. L. W. and C. H. D. contributed equally to this work.

*hammel@physics.osu.edu
†fyyang@physics.osu.edu

[1] Y. Kajiwara, K. Harii, S. Takahashi, J. Ohe, K. Uchida, M. Mizuguchi, H. Umezawa, H. Kawai, K. Ando, K. Takanashi, S. Maekawa, and E. Saitoh, Nature (London) **464**, 262 (2010).

[2] K. Uchida, S. Takahashi, K. Harii, J. Ieda, W. Koshibae, K. Ando, S. Maekawa, and E. Saitoh, Nature (London) **455**, 778 (2008).
[3] E. Saitoh, M. Ueda, H. Miyajima, and G. Tatara, Appl. Phys. Lett. **88**, 182509 (2006).
[4] F. D. Czeschka, L. Dreher, M. S. Brandt, M. Weiler, M. Althammer, I.-M. Imort, G. Reiss, A. Thomas, W. Schoch, W. Limmer, H. Huebl, R. Gross, and S. T. B. Goennenwein, Phys. Rev. Lett. **107**, 046601 (2011).
[5] R. Takahashi, R. Iguchi, K. Ando, H. Nakayama, T. Yoshino, and E. Saitoh, J. Appl. Phys. **111**, 07C307 (2012).
[6] K. Ando, Y. Kajiwara, S. Takahashi, S. Maekawa, K. Takemoto, M. Takatsu, and E. Saitoh, Phys. Rev. B **78**, 014413 (2008).
[7] C. W. Sandweg, Y. Kajiwara, A. V. Chumak, A. A. Serga, V. I. Vasyuchka, M. B. Jungfleisch, E. Saitoh, and B. Hillebrands, Phys. Rev. Lett. **106**, 216601 (2011).
[8] M. V. Costache, M. Sladkov, S. M. Watts, C. H. van der Wal, and B. J. van Wees, Phys. Rev. Lett. **97**, 216603 (2006).
[9] Y. Y. Sun, H. C. Chang, M. Kabatek, Y.-Y. Song, Z. H. Wang, M. Jantz, W. Schneider, M. Z. Wu, E. Montoya, B. Kardasz, B. Heinrich, S. G. E. te Velthuis, H. Schultheiss, and A. Hoffmann, Phys. Rev. Lett. **111**, 106601 (2013).
[10] O. Mosendz, V. Vlaminck, J. E. Pearson, F. Y. Fradin, G. E. W. Bauer, S. D. Bader, and A. Hoffmann, Phys. Rev. B **82**, 214403 (2010).
[11] E. Shikoh, K. Ando, K. Kubo, E. Saitoh, T. Shinjo, and M. Shiraishi, Phys. Rev. Lett. **110**, 127201 (2013).
[12] B. Heinrich, C. Burrowes, E. Montoya, B. Kardasz, E. Girt, Y.-Y. Song, Y. Y. Sun, and M. Z. Wu, Phys. Rev. Lett. **107**, 066604 (2011).
[13] S. Y. Huang, X. Fan, D. Qu, Y. P. Chen, W. G. Wang, J. Wu, T. Y. Chen, J. Q. Xiao, and C. L. Chien, Phys. Rev. Lett. **109**, 107204 (2012).
[14] A. Hoffmann, IEEE Trans. Magn. **49**, 5172 (2013).
[15] A. J. Hauser, J. R. Soliz, M. Dixit, R. E. A. Williams, M. A. Susner, B. Peters, L. M. Mier, T. L. Gustafson, M. D. Sumption, H. L. Fraser, P. M. Woodward, and F. Y. Yang, Phys. Rev. B **85**, 161201(R) (2012).
[16] A. J. Hauser, R. E. A. Williams, R. A. Ricciardo, A. Genc, M. Dixit, J. M. Lucy, P. M. Woodward, H. L. Fraser, and F. Y. Yang, Phys. Rev. B **83**, 014407 (2011).
[17] C. H. Du, R. Adur, H. L. Wang, A. J. Hauser, F. Y. Yang, and P. C. Hammel, Phys. Rev. Lett. **110**, 147204 (2013).
[18] B. Peters, A. Alfonsov, C. G. F. Blum, S. J. Hageman, P. M. Woodward, S. Wurmehl, B. Büchner, and F. Y. Yang, Appl. Phys. Lett. **103**, 162404 (2013).
[19] J. M. Lucy, A. J. Hauser, J. R. Soliz, M. Dixit, R. E. A. Williams, A. Holcombe, P. Morris, H. L. Fraser, D. W. McComb, P. M. Woodward, and F. Y. Yang, Appl. Phys. Lett. **103**, 042414 (2013).
[20] A. J. Hauser, J. M. Lucy, H. L. Wang, J. R. Soliz, A. Holcomb, P. Morris, P. M. Woodward, and F. Y. Yang, Appl. Phys. Lett. **102**, 032403 (2013).
[21] H. L. Wang, C. H. Du, Y. Pu, R. Adur, P. C. Hammel, and F. Y. Yang, Phys. Rev. B **88**, 100406(R) (2013).
[22] C. H. Du, H. L. Wang, Y. Pu, T. L. Meyer, P. M. Woodward, F. Y. Yang, and P. C. Hammel, Phys. Rev. Lett. **111**, 247202 (2013).
[23] D. D. Sarma, Proc. Indian Acad. Sci. **90**, 19 (1981).
[24] T. Kimura, J. Hamrle, and Y. Otani, Phys. Rev. B **72**, 014461 (2005).
[25] C. Hahn, G. de Loubens, O. Klein, M. Viret, V. V. Naletov, and J. Ben Youssef, Phys. Rev. B **87**, 174417 (2013).
[26] T. Kimura and Y. Otani, Phys. Rev. Lett. **99**, 196604 (2007).
[27] See Supplemental Material at http://link.aps.org/supplemental/10.1103/PhysRevLett.112.197201 for detailed analysis of spin pumping parameters.
[28] M. Farley, Rep. Prog. Phys. **61**, 755 (1998).
[29] P. Hansen, P. Röschmann, and W. Tolksdorf, J. Appl. Phys. **45**, 2728 (1974).
[30] L. Q. Liu, C.-F. Pai, Y. Li, H. W. Tseng, D. C. Ralph, and R. A. Buhrman, Science **336**, 555 (2012).
[31] C.-F. Pai, L. Q. Liu, Y. Li, H. W. Tseng, D. C. Ralph, and R. A. Buhrman, Appl. Phys. Lett. **101**, 122404 (2012).
[32] T. Tanaka, H. Kontani, M. Naito, T. Naito, D. S. Hirashima, K. Yamada, and J. Inoue, Phys. Rev. B **77**, 165117 (2008).
[33] M. Morota, Y. Niimi, K. Ohnishi, D. H. Wei, T. Tanaka, H. Kontani, T. Kimura, and Y. Otani, Phys. Rev. B **83**, 174405 (2011).
[34] S. S. Kalarickal, P. Krivosik, M. Z. Wu, C. E. Patton, M. L. Schneider, P. Kabos, T. J. Silva, and J. P. Nibarger, J. Appl. Phys. **99**, 093909 (2006).
[35] L. Q. Liu, R. A. Buhrman, and D. C. Ralph, arXiv:1111.3702.